Cell Systems

Report

# CTCF-Mediated Chromatin Loops between Promoter and Gene Body Regulate Alternative Splicing across Individuals

## Graphical Abstract

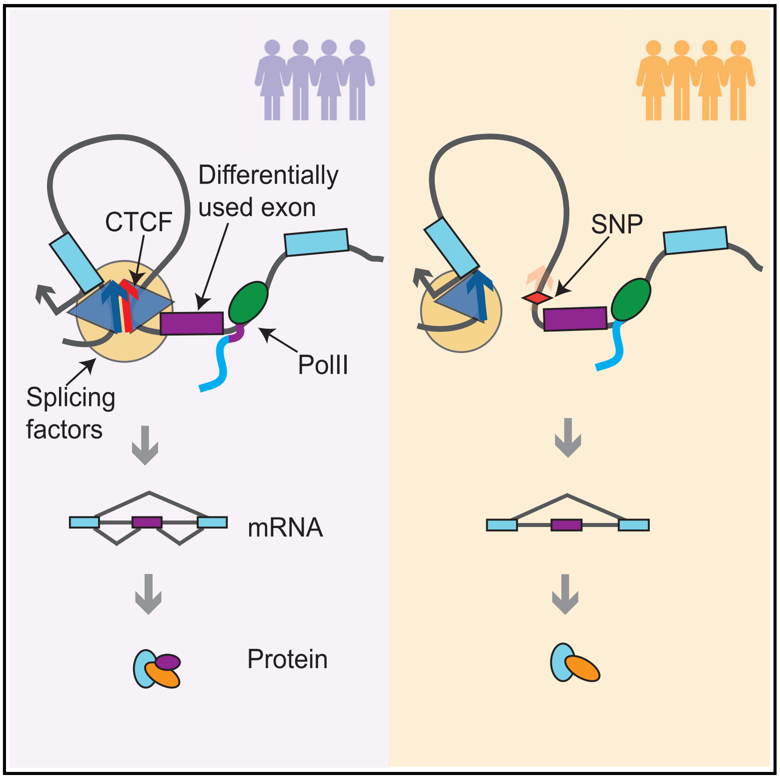

## Authors

Mariana Ruiz-Velasco, Manjeet Kumar, Mang Ching Lai, ..., Kyung-Min Noh, Toby J. Gibson, Judith B. Zaugg

## Correspondence

judith.zaugg@embl.de

## In Brief

The presence of CTCF-mediated intragenic chromatin loops regulates alternative splicing; this, in turn, may impact cellular decision making.

## Highlights

- CTCF-mediated intragenic looping can regulate alternative exon usage
- Genetic variation that affects CTCF looping leads to variation in splice isoforms
- Genes regulated by CTCF loops are involved in signaling and cellular stress response

Ruiz-Velasco et al., 2017, Cell Systems *5*, 1–10
December 27, 2017 © 2017 Published by Elsevier Inc.
https://doi.org/10.1016/j.cels.2017.10.018

CellPress

Please cite this article in press as: Ruiz-Velasco et al., CTCF-Mediated Chromatin Loops between Promoter and Gene Body Regulate Alternative Splicing across Individuals, Cell Systems (2017), https://doi.org/10.1016/j.cels.2017.10.018

Cell Systems
Report

# CTCF-Mediated Chromatin Loops between Promoter and Gene Body Regulate Alternative Splicing across Individuals

Mariana Ruiz-Velasco,[1] Manjeet Kumar,[1,6] Mang Ching Lai,[1,6] Pooja Bhat,[1,3] Ana Belen Solis-Pinson,[1,4] Alejandro Reyes,[2,5] Stefan Kleinsorg,[1] Kyung-Min Noh,[2] Toby J. Gibson,[1] and Judith B. Zaugg[1,7,*]
[1]Structural and Computational Biology, European Molecular Biology Laboratory, 69117 Heidelberg, Germany
[2]Genome Biology, European Molecular Biology Laboratory, 69117 Heidelberg, Germany
[3]Present address: Institute of Molecular Biotechnology of the Austrian Academy of Sciences, 1030 Vienna, Austria
[4]Present address: Department of Mathematics and Computer Science, Freie Universität Berlin, 14195 Berlin, Germany
[5]Present address: Biostatistics and Computational biology, Dana-Farber Cancer Institute, Boston, MA 02215, USA
[6]These authors contributed equally
[7]Lead Contact
*Correspondence: judith.zaugg@embl.de
https://doi.org/10.1016/j.cels.2017.10.018

## SUMMARY

**The CCCTC-binding factor (CTCF) is known to establish long-range DNA contacts that alter the three-dimensional architecture of chromatin, but how the presence of CTCF influences nearby gene expression is still poorly understood. Here, we analyze CTCF chromatin immunoprecipitation sequencing, RNA sequencing, and Hi-C data, together with genotypes from a healthy human cohort, and measure statistical associations between inter-individual variability in CTCF binding and alternative exon usage. We demonstrate that CTCF-mediated chromatin loops between promoters and intragenic regions are prevalent and that when exons are in physical proximity with their promoters, CTCF binding correlates with exon inclusion in spliced mRNA. Genome-wide, CTCF-bound exons are enriched for genes involved in signaling and cellular stress-response pathways. Structural analysis of three specific examples, checkpoint kinase 2 (CHK2), CDC-like kinase 3 (CLK3), and euchromatic histone-lysine N-methyltransferase (EHMT1), suggests that CTCF-mediated exon inclusion is likely to downregulate enzyme activity by disrupting annotated protein domains. In total, our study suggests that alternative exon usage is regulated by CTCF-dependent chromatin structure.**

## INTRODUCTION

In recent years, it has become evident that the three-dimensional (3D) organization of chromatin is highly regulated and likely to play important roles in gene regulation (Neems et al., 2016; Nora et al., 2012). A key factor for regulating the chromatin architecture is CTCF, a DNA-binding protein known to bring distant genomic elements into close spatial proximity by driving chromatin loop formation (Splinter et al., 2006; Yusufzai et al., 2004). The formation of these loops depends on the dimerization of two CTCF molecules in a convergent orientation that are bound to distant genomic loci (de Wit et al., 2015; Guo et al., 2015; Rao et al., 2014). To date most studies on 3D chromatin organization have focused on describing long-range gene-enhancer interactions (de Wit et al., 2015; Ji et al., 2016) or entire chromatin domains, and have largely remained descriptive with only a few examples that provide a mechanistic understanding for single loci reviewed in Ruiz-Velasco and Zaugg (2017). Functional insights have been particularly limited for shorter-range intragenic interactions, which are highly prevalent in many chromatin conformation experiments. By integrating multiple layers of genome-wide molecular phenotype data with genotypes, as well as curated genome and protein annotations, the results from our study indicate a functional role for CTCF-mediated intragenic chromatin looping in alternative splicing, particularly in regulating the inclusion of domains in proteins involved in signaling and cellular stress response.

## RESULTS

### Intragenic CTCF Motif Orientation Suggests Pervasive Promoter-Exon Looping

CTCF-mediated chromatin loops preferentially form between two convergently bound CTCF molecules (de Wit et al., 2015; Guo et al., 2015). Here we sought to assess the potential of intragenic CTCF loop formation by using its dependency on convergently oriented CTCF-binding sites. To do so, we quantified the distribution and orientation of intragenic CTCF motifs in genic regions grouped into four classes: promoter (±1 kb from transcription start site [TSS]), transcription termination site (TTS; ±1 kb), intronic regions upstream of exons (−2 kb from the exon 5′ end), and intronic regions downstream of exons (+2 kb from the exon 3′ end; STAR Methods: Annotation of Intragenic Loops). Next we scanned these regions for CTCF motifs, and defined their directionality as sense if both the motif and gene had the same orientation and antisense if vice versa.

We observe a bias for sense CTCF motifs at promoters ($p = 7 \times 10^{-7}$, binomial test) with a sharp increase 500 bp upstream

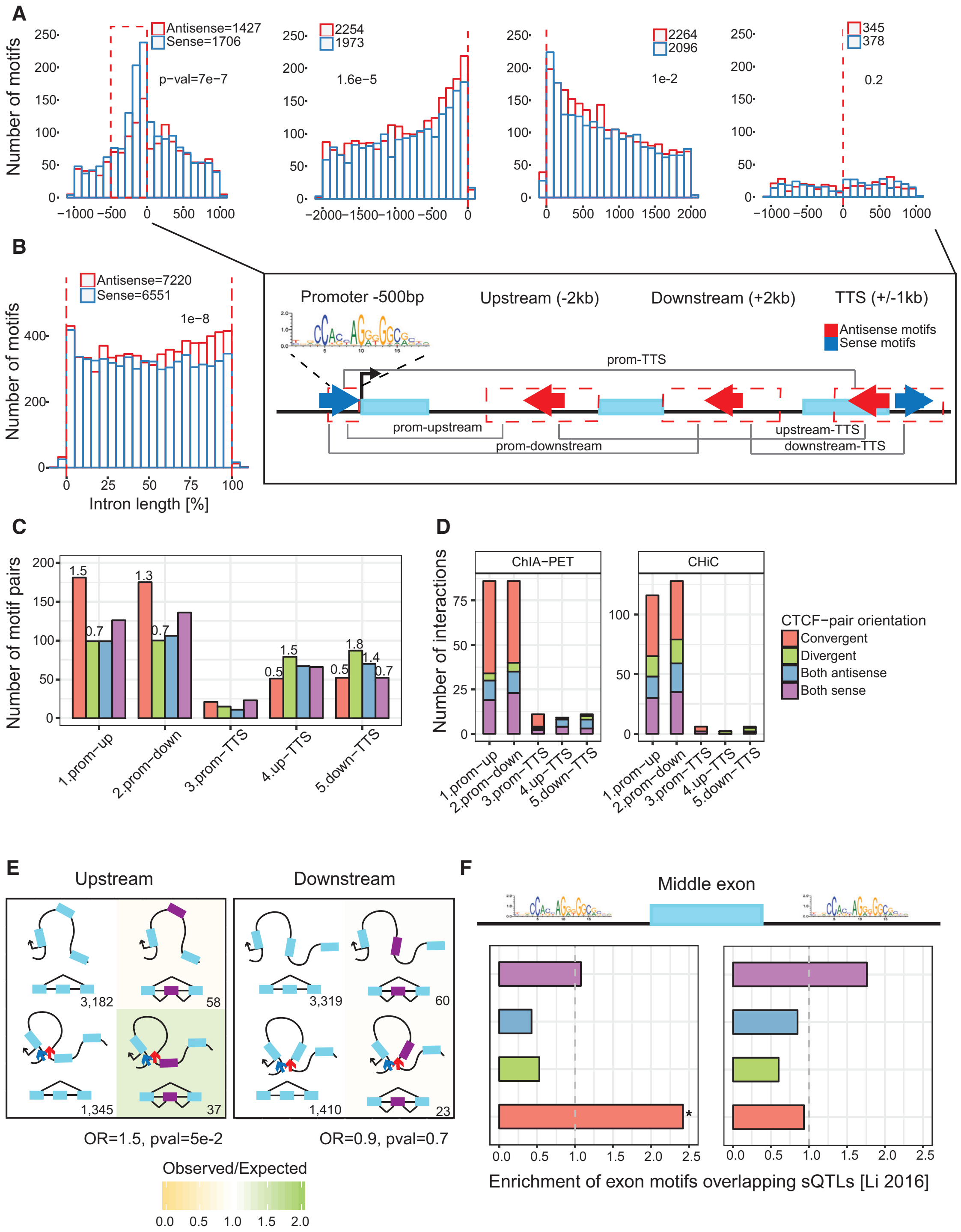

**Figure 1. CTCF Motifs Show Preferential Directionality along Transcripts**

(A and B) Distribution of CTCF motifs (overlapping with CTCF ChIP-seq peaks) in sense (blue) and antisense (red) orientation for four genic regions: promoter, upstream of exon, downstream of exon, and TTS (A; left to right; see also schematic), and along introns shown as percentage of their full length (B; see STAR Methods: Annotation of Intragenic Loops). The number of motifs is shown for each region; p values (p-val) are given for binomial tests.

(C) Orientation of CTCF interactions based on the motif pairs: promoter:exon-upstream (prom-up), promoter:exon-downstream (prom-down), promoter:TTS (prom-end), exon-upstream:TTS (up-end), and exon-downstream:TTS (down-end).

(D) Number of motif pairs with physical interaction based on ChIA-PET data of Rad21, H3K4me3 (Grubert et al., 2015), and CTCF (Tang et al., 2015) (left), and C-HiC (Mifsud et al., 2015) (right).

*(legend continued on next page)*

of the TSS ($p = 8.3 \times 10^{-11}$, dashed box in Figure 1A), while the region upstream and, to a lesser extent, downstream of exons contain preferentially antisense motifs ($p = 1.6 \times 10^{-5}$ and $1 \times 10^{-2}$, respectively; Figure 1A). Consistently, when considering all motifs across the intron we find an increase in antisense motifs at the 5′ end of exons (Figure 1B). TTS contain very few CTCF sites and no preference for any motif orientation. Notably, long non-coding RNAs showed no such pattern (Figure S1A), indicating that their 3D chromatin structure is fundamentally different from protein coding genes; thus, we excluded them from further analyses.

To evaluate whether these enrichments of sense and antisense motifs can form convergent CTCF pairs between promoter and exon-proximal regions, we grouped pairs of CTCF sites into "promoter:exon-upstream," "promoter:exon-downstream," "promoter:TTS," "exon-upstream:TTS," and "exon-downstream:TTS" pairs (schematic in Figure 1A), and classified each pair as "convergent," "divergent," "both sense," and "both antisense" depending on the relative orientation of the respective CTCF motifs. We found both classes of promoter-exon pairs strongly enriched for convergent configurations (odds ratio [OR] 1.5 and 1.3, $p = 3.4 \times 10^{-4}$ and $1.4 \times 10^{-2}$ for promoter:exon-upstream and promoter:exon-downstream, respectively; Fisher's exact test, Figure 1C). These findings suggest CTCF-mediated DNA loop formation between promoters and exon-proximal regions and allowed us to predict 181 promoter:exon-upstream loops involving 136 promoters with stringent thresholds, and 1,463 loops involving 956 promoters with less stringent criteria (lymphoblastoid cell line [LCL]-specific set; Figures S1B and S1C; STAR Methods: Annotation of Intragenic Loops).

To validate the loop predictions we used promoter capture-HiC (CHiC) and ChIA-PET data for Rad21, CTCF, and H3K4me3 (STAR Methods: Overlap with Chromatin Conformation Data) (Grubert et al., 2015; Mifsud et al., 2015; Tang et al., 2015). These contact maps captured 57% of the predicted loops. In accordance with our predictions, most contacts formed between promoters and exon-proximal regions with CTCF motifs in convergent orientation (OR 3.4, $p = 2.5 \times 10^{-9}$ for ChIA-PET and OR 1.6, $p = 4 \times 10^{-2}$ for CHiC; Fisher's exact test, Figure 1D).

Given this evidence of CTCF-mediated promoter-exon loops along with a previous report associating CTCF with alternative splicing at the *CD45* locus (Shukla et al., 2011), we hypothesized that CTCF might regulate alternative exon usage by bringing exons into close physical proximity with their promoter. Indeed, we found that exons whose upstream regions were predicted to loop to their promoter were enriched for differentially used exons (DUEs) across individuals (OR 1.5, $p = 5 \times 10^{-2}$, Fisher's exact test; Figure 1E and see below). No such enrichment was observed for promoter:exon-downstream loops.

A recent study found that genetic variants affecting alternative splicing across individuals (splicing quantitative trait loci [sQTLs]) often coincide with QTLs for CTCF (Li et al., 2016), suggesting a genome-wide role of CTCF in alternative splicing. We observed a strong enrichment for sQTLs to overlap with convergent promoter:exon-upstream CTCF pairs (OR 2.4, $p = 2 \times 10^{-2}$, Fisher's exact test; Figure 1F). Together, these results suggest a mechanistic involvement of CTCF-mediated promoter-exon looping in alternative exon usage.

## CTCF-Mediated Intragenic Chromatin Loops Regulate Alternative Exon Usage

One prediction of such a mechanism is that exons which can form a loop with their promoter are more likely differentially used than non-looping exons. Thus we expect (1) that changes in CTCF binding across individuals correlate with differential exon usage for exons that can form a loop with their promoters (convergent promoter:exon pairs), and (2) that such a correlation does not exist for other exons.

We employed CTCF chromatin immunoprecipitation sequencing (ChIP-seq) and matching RNA sequencing (RNA-seq) data for 18 individuals (Kasowski et al., 2013) to calculate the variation on CTCF binding and exon usage (Figure 2A; STAR Methods: Identification of Differentially Used Exons). In brief, we used DEXSeq (Anders et al., 2012) to identify DUEs from the set of middle exons expressed in LCLs (62,663), which resulted in 2,081 DUEs at a 10% false discovery rate (FDR) (Figures S2A–S2D). CTCF binding at these DUEs was quantified by averaging the signal of CTCF within 2 kb of the respective exon boundaries (upstream and downstream; STAR Methods: CTCF Correlation with DUEs). For each individual we then calculated $\log_2$ fold-change values of differential exon usage and CTCF binding with respect to the median across all individuals. These ratios were then assessed by Spearman correlation to investigate the relationship between CTCF binding and exon usage (Figure 2B; STAR Methods: CTCF Correlation with DUEs).

The correlations were generally not driven by outliers, as shown for a few representative examples (Figure 2C). Notably, we find that exons with upstream convergent pairs show a strong bias toward positive correlations, whereas the correlations of CTCF with non-looping exons were indistinguishable from empirical correlations (100 permutations; Figures 2D and S2E).

In summary, these results support the model in which CTCF-dependent alternative exon usage is mediated by intragenic promoter:exon loops. Interestingly, the evidence holds only for promoter:exon-upstream pairs.

## Allele-Specific Analysis Confirms the Model of CTCF-Dependent Alternative Exon Usage Mediated by DNA Interactions

To directly test the link between chromatin loop formation and exon usage, we sought to use genetic variation to quantify the allelic fractions of chromatin contact frequencies (data taken from Rao et al., 2014), CTCF binding, and exonic expression.

(E) Schematic of contingency table for testing the association of differentially used exons (DUE) and promoter-exon:upstream (left) and promoter-exon:downstream (right) loops. The p values (pval) are given for Fisher's exact test; OR, odds ratio. Background color represents ratio of observed versus expected events. DUEs are calculated based on RNA-seq data from LCLs of 18 individuals (STAR Methods: Identification of Differentially Used Exons).

(F) Enrichment of sQTLs (FDR = 10%) (Li et al., 2016) overlapping with a particularly oriented CTCF motif (± 20 bp from midpoint) upstream (left) or downstream (right) of a middle exon (*$p < 0.05$, Fisher's exact test).

See also Figure S1.

Please cite this article in press as: Ruiz-Velasco et al., CTCF-Mediated Chromatin Loops between Promoter and Gene Body Regulate Alternative Splicing across Individuals, Cell Systems (2017), https://doi.org/10.1016/j.cels.2017.10.018

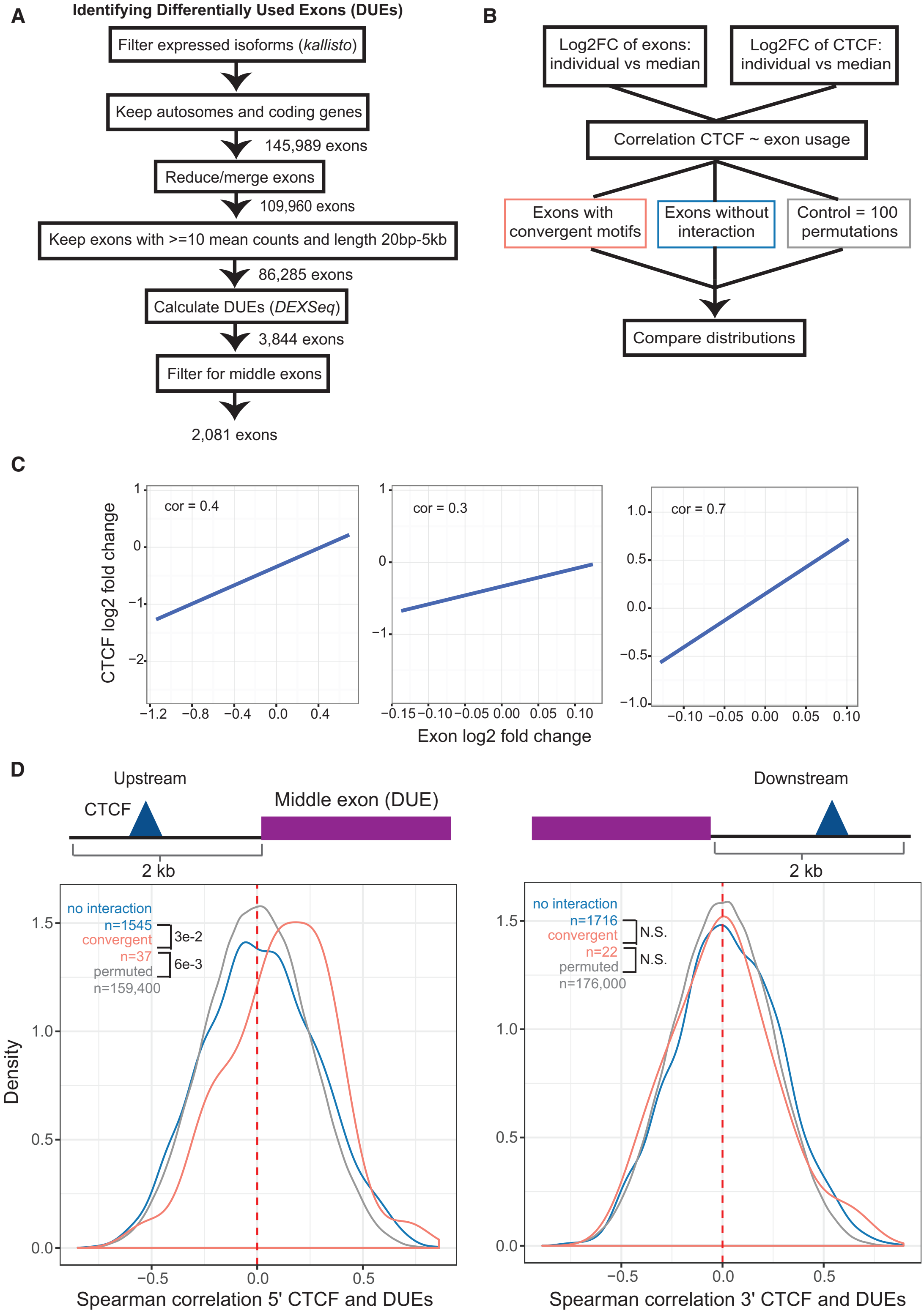

**Figure 2. Relationship between CTCF and Differentially Used Exons**

(A) Workflow used to identify DUEs across individuals.

(B) Workflow used to calculate the correlations between CTCF binding (ChIP-seq) and exon usage (RNA-seq) across 18 individuals. Three groups were considered: exon-promoter pairs with convergent motifs (red), without motifs (blue), and 100 permutations (gray).

(C) The $\log_2$ fold change of CTCF binding and exon usage across individuals are shown for three examples.

(legend continued on next page)

To do so, we performed a joint allele-specific analysis at heterozygous SNPs that overlapped with a CTCF peak within 2 kb upstream or downstream of an exon boundary and considered all events that showed an allelic bias for CTCF binding at a nominal p value of 0.05 (STAR Methods: Allele-Specific Analysis of CTCF Binding).

We observed a significant positive correlation between the allelic fractions of CTCF and exon expression level for upstream and, to a lesser extent, downstream regions (Pearson's R = 0.5 and 0.3, respectively; top panel in Figure 3A). As a more robust quantification we classified the exons according to the directionality of the allelic bias in CTCF binding and assessed differences in exon allelic fractions between the two groups by a t test (bottom panel in Figures 3A and S3A). This revealed a significant association only for the CTCF sites upstream of the exon.

When further grouping the exons into convergent and non-looping (any other configuration), we found a strong association between the allelic fractions of CTCF and exon usage for exons in promoter:exon-upstream loops and not for others (Figure 3C, left). This was even more pronounced for the association of exons with Hi-C allelic biases (Figures 3B, 3C, and S3B; STAR Methods: Allele-Specific Analysis of CTCF Binding). In summary, we found a consistent allelic bias in CTCF, Hi-C, and exon usage for exons in promoter:exons-upstream pairs in convergent orientation, but not for other exons, which indicates that it is not the loss of CTCF per se, but the loss of a CTCF-mediated promoter interaction, that regulates exon usage—potentially through changes in the chromatin environment (Figure 3B).

To experimentally validate these global correlations, we performed 4C-seq (circular chromatin conformation capture combined with high-throughput sequencing) experiments for six individuals in a highly expressed gene that has a DUE (exon 5) in a predicted promoter:exon-upstream loop, and exhibits high correlation between CTCF and its DUE (*THRAP3*). We found extensive chromatin interactions between the *THRAP3* promoter and several regions within the gene (Figure S3C). Notably, exon 5 showed a higher 4C-seq signal in individuals with more inclusion of the exon (Figure 3D). No such difference in 4C-seq count was observed for other exons (Figure S3D).

The findings above exemplify how a genetic variant can disrupt CTCF binding upstream of an exon, which in turn prevents the exon from being included in the transcript.

### Functional Consequences of Genes and Exons with Predicted Promoter-Exon Loops

Finally, we sought to assess the potential impact of CTCF-loop-regulated exons on the protein level. The analyses were carried out for all exons involved in a predicted loop, regardless of their expression status in LCLs (referred to as "unbiased set"), and corroborated with the LCL-specific set used in the analysis above (STAR Methods: Functional Analyses). Corroborating the CTCF-mediated splicing predictions, we found that for a large proportion of the loop-regulated exons a known protein isoform exists that lacks the respective exon (Figure 4A). These exons are more likely than others to overlap fully with a missing region of a known alternative protein isoform (1.6-fold, $p = 4.2 \times 10^{-2}$, Fisher's exact test), suggesting that the loop-regulated exons are indeed contributing to generate distinct protein isoforms.

We found that loop-regulated exons tend to overlap with a Pfam protein domain more than expected (OR 1.8, $p < 2.2 \times 10^{-16}$ and OR 3.0, $p < 2.2 \times 10^{-16}$ for LCL-specific exons; Fisher's exact test), and in particular with kinase domains (OR = 2.3 and 5.1; adjusted p value $2.2 \times 10^{-6}$ and $3.0 \times 10^{-4}$, respectively). A gene ontology analysis on the genes containing loop-regulated exons revealed a strong enrichment for terms related to "signaling" and "cellular response to stimuli" (Figures 4B, S4A, and S4C). Consequently, we found that genes containing loop-regulated exons are predominantly associated with membrane, cell-periphery, or cell-projection structures (Figure S4B).

In Figures 4C–4E we showcase three well-studied proteins where the looped exon is absent from at least one of the known isoforms: checkpoint kinase 2 (CHK2) has over 90 splice variants, 13 of which are annotated in Swiss-Prot/UniProt, and for five of them the loop-regulated exon is missing (Figure 4C). CDC-like kinase CLK3, involved in regulating the spliceosome, has a known catalytically inactive isoform, which is caused by a premature stop codon upon exclusion of exon 4 (Duncan et al., 1995; Hanes et al., 1994), which is predicted to be loop regulated (Figure 4D). The ratio of inclusion of exon 4 has been proposed to control the differentiation process in multiple cell types (García-Sacristán et al., 2005). Finally, euchromatic histone-lysine N-methyltransferase 1 (EHMT1), involved in mono- and dimethylation of H3K9, has four isoforms described in Swiss-Prot, two of which involve a loop-regulated exon. Isoform 2 lacks the whole EHMT1 protein when excluding loop-regulated exon 2 as a consequence of a premature stop codon, while isoform 4 skips the loop-regulated exon 26, thereby removing half of the SET domain (Figure 4E), presumably eliminating the catalytic activity while retaining the chromatin location and histone tail-binding properties of the protein.

Overall, these examples illustrate that CTCF-mediated intragenic loop formation can impact on protein function, particularly disrupting kinase domains and potentially playing a role in cellular signaling and response to stimuli.

## DISCUSSION

Chromatin topology and function are tightly linked to ensure proper genomic regulation, but only few studies have shown a direct link between chromatin organization and gene regulation (Ruiz-Velasco and Zaugg, 2017). CTCF has been shown to regulate alternative exon usage at the *CD45* locus by Shukla

(D) Distribution of Spearman correlations between the $\log_2$ fold change of DUEs and CTCF (as shown in C) are shown for CTCF bound upstream (left) and downstream (right) of the exon. The correlation values are grouped into convergent (red; n = 37 and n = 22 upstream and downstream, respectively), exons without motif pairs (blue; n = 1,545 and n = 1,716), and obtained from 100 sets of correlations using permuted sample labels (gray; n = 159,400 and n = 176,000). Convergently oriented upstream exons show a significant shift toward positive correlations (p < 0.05 are reported in the figure and otherwise stated as non-significant [N.S.], Wilcoxon rank-sum test).
See also Figure S2.

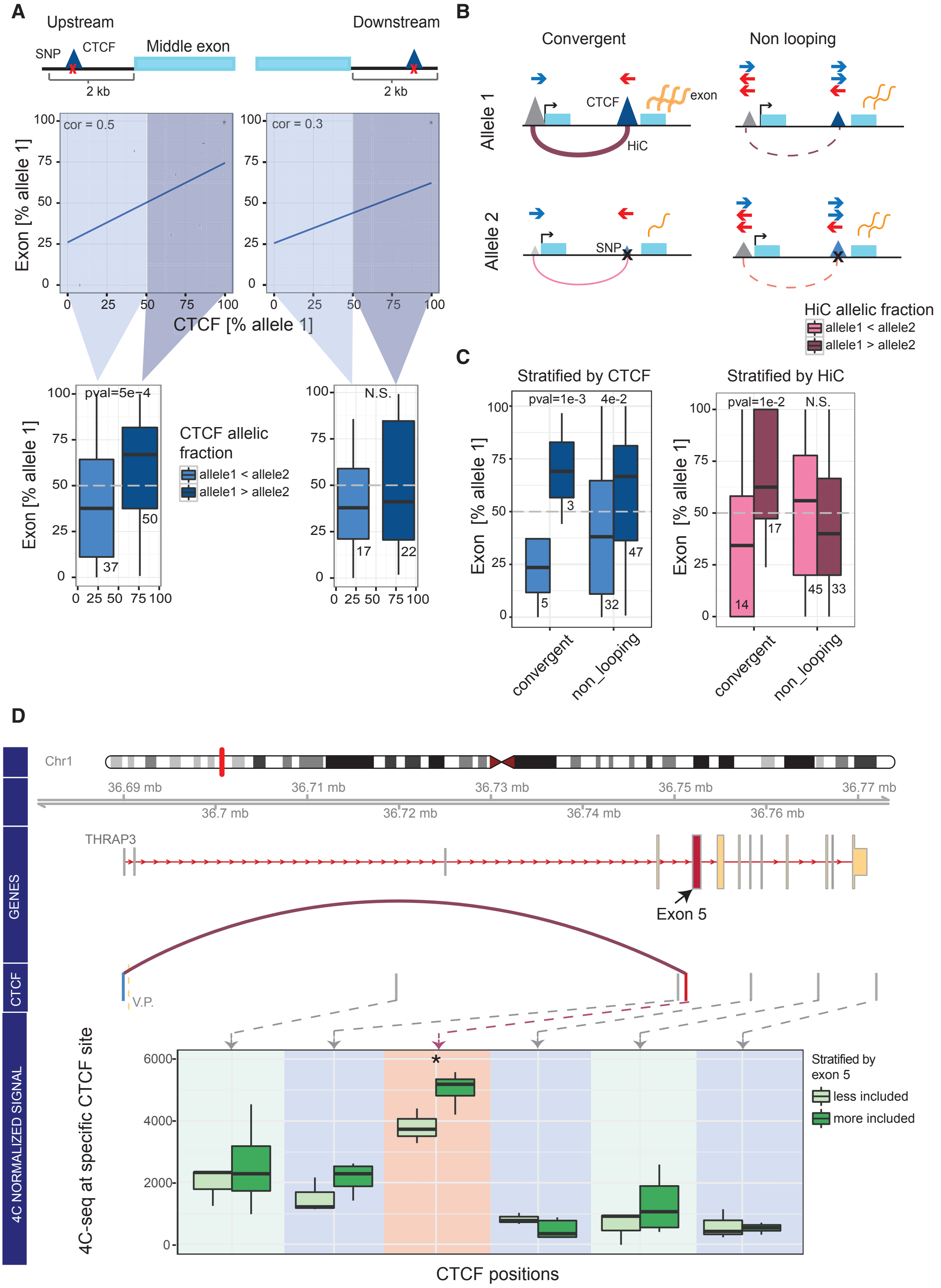

**Figure 3. Genetic Variants Jointly Affect CTCF Binding and Exon Inclusion**

(A) Pearson correlations of allelic fraction estimates of exon expression levels (RNA-seq) and CTCF signal (ChIP-seq) for heterozygous SNPs contained within the CTCF peaks are shown (n = 14 individuals). The schematic shows the window used for identifying allele-specific CTCF peaks. Plots show the percentage of reads mapping to allele 1.

*(legend continued on next page)*

and colleagues, whereby CTCF bound downstream of the exon was proposed to slow down RNA polymerase II (Pol II) by creating a "roadblock," consequently allowing weak splicing sites to be recognized by the spliceosome (Shukla et al., 2011). However, the roadblock model does not take into account the major role of CTCF in chromatin 3D organization. Our data suggest an additional role for CTCF bound upstream of an exon to regulate its inclusion (Figure 4F), thus encompassing 3D chromatin organization by CTCF as a novel mechanism for splicing regulation in addition to the previously proposed roadblock model. Thus our study provides a functional link between intragenic chromatin 3D organization and splicing regulation.

We speculate that this mechanism works via: (1) slowing down RNA Pol II elongation, a well-established mechanism in splicing regulation (Fong et al., 2014; Jonkers et al., 2014; Oesterreich et al., 2016; Shukla et al., 2011), and (2) increasing the local concentration of splicing-promoting factors at the exon. Since CTCF-binding sites represent boundary elements for the cohesin-mediated loop extrusion process (Haarhuis et al., 2017), it is possible that such cohesin-CTCF loop boundary acts as a roadblock for slowing down RNA Pol II elongation, hence affecting splicing. Furthermore, splicing factors are known to localize at promoters (Huang et al., 2012; Kornblihtt et al., 2013; Mikula et al., 2013) and could therefore regulate splicing at distal exons when brought into close proximity by chromatin looping. In support of this, it has been shown that the chromatin environment upstream of alternative exons can affect exon inclusion through splicing factor recruitment (Agirre et al., 2015; Curado et al., 2015; Mercer et al., 2013). Indeed, we found a correlation between signal strengths of histone marks that characterize gene promoter activities (H3K4me3, H3K27ac) and exon inclusion only in loop-regulated exons (Figure S2F). Altogether, the results here demonstrate the intricate relationship between chromatin structure, promoter state, and splicing regulation.

However, while there is clear evidence that CTCF looping affects alternative exon usage, our study faces several limitations: the identification of novel splicing mechanisms at the chromatin level is limited by both the resolution and coverage of the datasets used in our analyses, and incomplete gene and protein isoform annotations. It should also be noted that various other mechanisms are likely to function in parallel or in addition to the one proposed here, as reflected by the overall moderate effect sizes reported in this study. For example, CTCF-RNA interactions (Kung et al., 2015; Saldaña-Meyer et al., 2014) and/or the competition between intragenic enhancer RNA expression could form additional levels of splicing regulation, even though we did our best to avoid masking the effects of CTCF looping on splicing by alternative transcription initiation events (i.e., using our CAGE filter; STAR Methods: Annotation of Intragenic Loops). Finally, despite the strong evidence obtained from genetic variation and the validation using 4C-seq, we have not tested the mechanism biochemically by perturbing a CTCF-binding site.

This study provides a framework for further investigating alternative isoform usage in the context of diseases and development. For instance, since CTCF binding is DNA-methylation sensitive, DNA-methylation status in cancer or across development could regulate alternative exon usage via CTCF-binding sites. Thus, our model opens up the possibility that epigenomic changes that affect chromatin 3D structures may play roles in fine-tuning alternative splicing.

## STAR★METHODS

Detailed methods are provided in the online version of this paper and include the following:

## SUPPLEMENTAL INFORMATION

Supplemental Information includes four figures and can be found with this article online at https://doi.org/10.1016/j.cels.2017.10.018.

## AUTHOR CONTRIBUTIONS

Conceptualization, J.B.Z. and M.R.-V.; Software and Formal Analysis, M.R.-V. (genomic analyses), M.K. (functional protein analyses), P.B., A.B.S.-P., A.R., and S.K. (contributed to the analyses); Methodology, M.R.-V., J.B.Z., M.C.L., and K.M.N.; Validation, M.C.L. and M.R.-V.; Writing – Original Draft, J.B.Z., M.R.-V., and M.K.; Writing – Review and Editing, J.B.Z., M.R.-V., M.K., and M.C.L.; Visualization, M.R.V., M.K., M.C.L., and J.B.Z.; Supervision, J.B.Z., K.-M.N., and T.J.G.

(B) Schematic summarizing the results of the allele-specific analysis. When the exon has an exon-upstream CTCF motif in a convergent configuration with its promoter, we observe a positive correlation between CTCF, exon usage, and HiC signal. No such correlation is observed for any other (non-looping) exon-promoter orientation (Figures S3A and S3B).

(C) Exon allelic fraction stratified by binned CTCF allelic fraction (n = 14 individuals; left) and binned HiC allelic fraction (n = 1 individual; right) (allele 1 > allele 2 and vice versa) are shown grouped by the configuration of the exon-promoter motif pair.

(D) 4C-seq signals in 6 individuals stratified by amount of inclusion ("more" or "less") of exon 5 for *THRAP3* are shown for each CTCF site along the transcript. The CTCF peaks predicted to form a loop with the promoter (according to their highest scoring motif) are shown in blue for sense and red for antisense. Exon 5 is highlighted in red (V.P., viewpoint; *$p < 0.05$).

See also Figure S3.

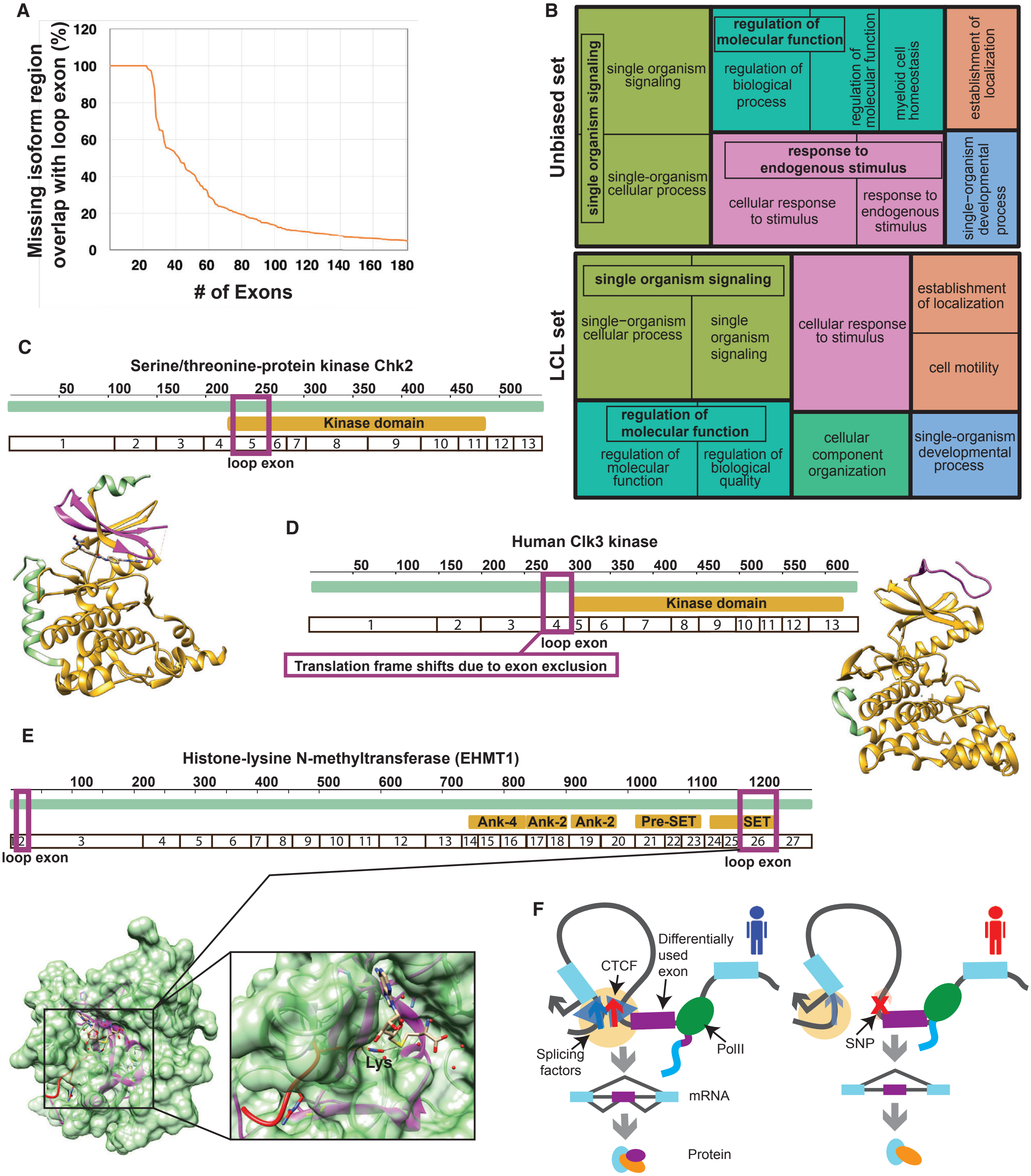
A
Missing isoform region overlap with loop exon (%)
0
20
40
60
80
100
120
20 40 60 80 100 120 140 160 180
# of Exons
B
Unbiased set
single organism signaling
single organism signaling
single-organism cellular process
regulation of molecular function
regulation of biological process
regulation of molecular function
myeloid cell homeostasis
establishment of localization
response to endogenous stimulus
cellular response to stimulus
response to endogenous stimulus
single-organism developmental process
LCL set
single organism signaling
single-organism cellular process
single organism signaling
cellular response to stimulus
establishment of localization
cell motility
regulation of molecular function
regulation of molecular function
regulation of biological quality
cellular component organization
single-organism developmental process
C
Serine/threonine-protein kinase Chk2
50 100 150 200 250 300 350 400 450 500
Kinase domain
1 2 3 4 5 6 7 8 9 10 11 12 13
loop exon
D
Human Clk3 kinase
50 100 150 200 250 300 350 400 450 500 550 600
Kinase domain
1 2 3 4 5 6 7 8 9 10 11 12 13
loop exon
Translation frame shifts due to exon exclusion
E
Histone-lysine N-methyltransferase (EHMT1)
100 200 300 400 500 600 700 800 900 1000 1100 1200
Ank-4 Ank-2 Ank-2 Pre-SET SET
2 3 4 5 6 7 8 9 10 11 12 13 14 15 16 17 18 19 20 21 22 23 24 25 26 27
loop exon
loop exon
Lys
F
CTCF
Differentially used exon
Splicing factors
PolII
mRNA
Protein
SNP

**Figure 4. Influence of CTCF-Mediated Intragenic Loop Exon on Protein Function**

(A) The cumulative distribution of overlaps between looping exons (based on the unbiased set of CTCF motif pairs; STAR Methods: Functional Analyses) and missing regions of known protein isoforms are shown (as percentage of the missing region).

(B) Treemap representations from Revigo (Supek et al., 2011) showing significantly enriched biological processes (top 10) for the genes containing loop exons in the unbiased (upper panel) and the LCL-specific set (bottom panel).

(C–E) Visualization of exon structure, primary sequence, and 3D structure for selected loop exon gene products. Loop exons are colored in magenta on the primary and 3D structure. (C) Human checkpoint kinase CHK2 (UniProt: O96017; PDB: 2YCF): The kinase domain is affected by the looping exon (exon 5). (D)

(legend continued on next page)

## ACKNOWLEDGMENTS

We thank Christian Arnold for help with using *SNPhood*, and Christian Valdes-Quezada for advice on 4C-seq. We are thankful for the discussions and critical comments from Erez Lieberman-Aiden, Suhas Rao, Job Dekker, Esa Pitkanen, and Ricardo Saldaña-Meyer. We acknowledge the Genecore facility and funding by EMBL. M.K. is funded by the Humboldt Foundation.

Received: July 29, 2016
Revised: August 2, 2017
Accepted: October 27, 2017
Published: November 29, 2017

## REFERENCES

Agirre, E., Bellora, N., Alló, M., Pagès, A., Bertucci, P., Kornblihtt, A.R., and Eyras, E. (2015). A chromatin code for alternative splicing involving a putative association between CTCF and HP1α proteins. BMC Biol. *13*, 31.

Anders, S., Reyes, A., and Huber, W. (2012). Detecting differential usage of exons from RNA-seq data. Genome Res. *22*, 2008–2017.

Arnold, C., Bhat, P., and Zaugg, J.B. (2016). SNPhood: investigate, quantify and visualise the epigenomic neighbourhood of SNPs using NGS data. Bioinformatics *32*, 2359–2360.

Bateman, A., Coin, L., Durbin, R., Finn, R.D., Hollich, V., Griffiths-Jones, S., Khanna, A., Marshall, M., Moxon, S., Sonnhammer, E.L.L., et al. (2004). The Pfam protein families database. Nucleic Acids Res. *32*, D138–D141.

Berman, H.M., Westbrook, J., Feng, Z., Gilliland, G., Bhat, T.N., Weissig, H., Shindyalov, I.N., and Bourne, P.E. (2000). The Protein Data Bank. Nucleic Acids Res. *28*, 235–242.

Bray, N.L., Pimentel, H., Melsted, P., and Pachter, L. (2016). Near-optimal probabilistic RNA-seq quantification. Nat. Biotechnol. *34*, 525–527.

Cunningham, F., Amode, M.R., Barrell, D., Beal, K., Billis, K., Brent, S., Carvalho-Silva, D., Clapham, P., Coates, G., Fitzgerald, S., et al. (2015). Ensembl 2015. Nucleic Acids Res. *43*, D662–D669.

Curado, J., Iannone, C., Tilgner, H., Valcárcel, J., and Guigó, R. (2015). Promoter-like epigenetic signatures in exons displaying cell type-specific splicing. Genome Biol. *16*, 236.

Derrien, T., Johnson, R., Bussotti, G., Tanzer, A., Djebali, S., Tilgner, H., Guernec, G., Martin, D., Merkel, A., Knowles, D.G., et al. (2012). The GENCODE v7 catalog of human long noncoding RNAs: analysis of their gene structure, evolution, and expression. Genome Res. *22*, 1775–1789.

Duncan, P.I., Howell, B.W., Marius, R.M., Drmanic, S., Douville, E.M., and Bell, J.C. (1995). Alternative splicing of STY, a nuclear dual specificity kinase. J. Biol. Chem. *270*, 21524–21531.

Fang, H. (2014). dcGOR: an R package for analysing ontologies and protein domain annotations. PLoS Comput. Biol. *10*, e1003929.

FANTOM Consortium and the RIKEN PMI and CLST (DGT), Forrest, A.R.R., Kawaji, H., Rehli, M., Baillie, J.K., de Hoon, M.J.L., Haberle, V., Lassmann, T., Kulakovskiy, I.V., Lizio, M., et al. (2014). A promoter-level mammalian expression atlas. Nature *507*, 462–470.

Fong, N., Kim, H., Zhou, Y., Ji, X., Qiu, J., Saldi, T., Diener, K., Jones, K., Fu, X.-D., and Bentley, D.L. (2014). Pre-mRNA splicing is facilitated by an optimal RNA polymerase II elongation rate. Genes Dev. *28*, 2663–2676.

García-Sacristán, A., Fernández-Nestosa, M.J., Hernández, P., Schvartzman, J.B., and Krimer, D.B. (2005). Protein kinase clk/STY is differentially regulated during erythroleukemia cell differentiation: a bias toward the skipped splice variant characterizes postcommitment stages. Cell Res. *15*, 495–503.

Grubert, F., Zaugg, J.B., Kasowski, M., Ursu, O., Spacek, D.V., Martin, A.R., Greenside, P., Srivas, R., Phanstiel, D.H., Pekowska, A., et al. (2015). Genetic control of chromatin states in humans involves local and distal chromosomal interactions. Cell *162*, 1051–1065.

Guo, Y., Xu, Q., Canzio, D., Shou, J., Li, J., Gorkin, D.U., Jung, I., Wu, H., Zhai, Y., Tang, Y., et al. (2015). CRISPR inversion of CTCF sites alters genome topology and enhancer/promoter function. Cell *162*, 900–910.

Haarhuis, J.H.I., van der Weide, R.H., Blomen, V.A., Yáñez-Cuna, J.O., Amendola, M., van Ruiten, M.S., Krijger, P.H.L., Teunissen, H., Medema, R.H., van Steensel, B., et al. (2017). The cohesin release factor WAPL restricts chromatin loop extension. Cell *169*, 693–707.e14.

Hanes, J., von der Kammer, H., Klaudiny, J., and Scheit, K.H. (1994). Characterization by cDNA cloning of two new human protein kinases. Evidence by sequence comparison of a new family of mammalian protein kinases. J. Mol. Biol. *244*, 665–672.

Huang, Y., Li, W., Yao, X., Lin, Q.-J., Yin, J.-W., Liang, Y., Heiner, M., Tian, B., Hui, J., and Wang, G. (2012). Mediator complex regulates alternative mRNA processing via the MED23 subunit. Mol. Cell *45*, 459–469.

Ji, X., Dadon, D.B., Powell, B.E., Fan, Z.P., Borges-Rivera, D., Shachar, S., Weintraub, A.S., Hnisz, D., Pegoraro, G., Lee, T.I., et al. (2016). 3D chromosome regulatory landscape of human pluripotent cells. Cell Stem Cell *18*, 262–275.

Jonkers, I., Kwak, H., and Lis, J.T. (2014). Genome-wide dynamics of Pol II elongation and its interplay with promoter proximal pausing, chromatin, and exons. Elife *3*, e02407.

Kamburov, A., Stelzl, U., Lehrach, H., and Herwig, R. (2013). The ConsensusPathDB interaction database: 2013 update. Nucleic Acids Res. *41*, D793–D800.

Kasowski, M., Kyriazopoulou-Panagiotopoulou, S., Grubert, F., Zaugg, J.B., Kundaje, A., Liu, Y., Boyle, A.P., Zhang, Q.C., Zakharia, F., Spacek, D.V., et al. (2013). Extensive variation in chromatin states across humans. Science *342*, 750–752.

Kornblihtt, A.R., Schor, I.E., Alló, M., Dujardin, G., Petrillo, E., and Muñoz, M.J. (2013). Alternative splicing: a pivotal step between eukaryotic transcription and translation. Nat. Rev. Mol. Cell Biol. *14*, 153–165.

Kung, J.T., Kesner, B., An, J.Y., Ahn, J.Y., Cifuentes-Rojas, C., Colognori, D., Jeon, Y., Szanto, A., del Rosario, B.C., Pinter, S.F., et al. (2015). Locus-specific targeting to the X chromosome revealed by the RNA interactome of CTCF. Mol. Cell *57*, 361–375.

Langmead, B., and Salzberg, S.L. (2012). Fast gapped-read alignment with Bowtie 2. Nat. Methods *9*, 357–359.

Lawrence, M., Huber, W., Pagès, H., Aboyoun, P., Carlson, M., Gentleman, R., Morgan, M.T., and Carey, V.J. (2013). Software for computing and annotating genomic ranges. PLoS Comput. Biol. *9*, e1003118.

Li, Y., Huang, W., Niu, L., Umbach, D.M., Covo, S., and Li, L. (2013). Characterization of constitutive CTCF/cohesin loci: a possible role in establishing topological domains in mammalian genomes. BMC Genomics *14*, 553.

Li, Y.I., van de Geijn, B., Raj, A., Knowles, D.A., Petti, A.A., Golan, D., Gilad, Y., and Pritchard, J.K. (2016). RNA splicing is a primary link between genetic variation and disease. Science *352*, 600–604.

Mercer, T.R., Edwards, S.L., Clark, M.B., Neph, S.J., Wang, H., Stergachis, A.B., John, S., Sandstrom, R., Li, G., Sandhu, K.S., et al. (2013). DNase I-hypersensitive exons colocalize with promoters and distal regulatory elements. Nat. Genet. *45*, 852–859.

Mifsud, B., Tavares-Cadete, F., Young, A.N., Sugar, R., Schoenfelder, S., Ferreira, L., Wingett, S.W., Andrews, S., Grey, W., Ewels, P.A., et al. (2015). Mapping long-range promoter contacts in human cells with high-resolution capture Hi-C. Nat. Genet. *47*, 598–606.

Mikula, M., Bomsztyk, K., Goryca, K., Chojnowski, K., and Ostrowski, J. (2013). Heterogeneous nuclear ribonucleoprotein (HnRNP) K genome-wide

Human CLK3 kinase (UniProt: P49761; PDB: 2EU9): The loop exon (exon 4) is alternatively used in protein isoforms that then lack the entire kinase domain. (E) Euchromatic histone-lysine N-methyltransferase (EHMT1) (UniProt: Q9H9B1; PDB: 3HNA): loop exons 2 and 26 produce isoforms that affect protein function. (F) Schematic of the proposed mechanism.
See also Figure S4.

binding survey reveals its role in regulating 3′-end RNA processing and transcription termination at the early growth response 1 (EGR1) gene through XRN2 exonuclease. J. Biol. Chem. *288*, 24788–24798.

Neems, D.S., Garza-Gongora, A.G., Smith, E.D., and Kosak, S.T. (2016). Topologically associated domains enriched for lineage-specific genes reveal expression-dependent nuclear topologies during myogenesis. Proc. Natl. Acad. Sci. USA *113*, E1691–E1700.

Nora, E.P., Lajoie, B.R., Schulz, E.G., Giorgetti, L., Okamoto, I., Servant, N., Piolot, T., van Berkum, N.L., Meisig, J., Sedat, J., et al. (2012). Spatial partitioning of the regulatory landscape of the X-inactivation centre. Nature *485*, 381–385.

Oesterreich, F.C., Herzel, L., Straube, K., Hujer, K., Howard, J., and Neugebauer, K.M. (2016). Splicing of nascent RNA coincides with intron exit from RNA polymerase II. Cell *165*, 372–381.

Quinlan, A.R., and Hall, I.M. (2010). BEDTools: a flexible suite of utilities for comparing genomic features. Bioinformatics *26*, 841–842.

Rao, S.S.P., Huntley, M.H., Durand, N.C., Stamenova, E.K., Bochkov, I.D., Robinson, J.T., Sanborn, A.L., Machol, I., Omer, A.D., Lander, E.S., et al. (2014). A 3D map of the human genome at kilobase resolution reveals principles of chromatin looping. Cell *159*, 1665–1680.

Ruiz-Velasco, M., and Zaugg, J.B. (2017). Structure meets function: how chromatin organisation conveys functionality. Curr. Opin. Syst. Biol. *1*, 129–136.

Saldaña-Meyer, R., González-Buendía, E., Guerrero, G., Narendra, V., Bonasio, R., Recillas-Targa, F., and Reinberg, D. (2014). CTCF regulates the human p53 gene through direct interaction with its natural antisense transcript, Wrap53. Genes Dev. *28*, 723–734.

Shukla, S., Kavak, E., Gregory, M., Imashimizu, M., Shutinoski, B., Kashlev, M., Oberdoerffer, P., Sandberg, R., and Oberdoerffer, S. (2011). CTCF-promoted RNA polymerase II pausing links DNA methylation to splicing. Nature *479*, 74–79.

Soneson, C., Matthes, K.L., Nowicka, M., Law, C.W., and Robinson, M.D. (2016). Isoform prefiltering improves performance of count-based methods for analysis of differential transcript usage. Genome Biol. *17*, 12.

Splinter, E., Heath, H., Kooren, J., Palstra, R.-J., Klous, P., Grosveld, F., Galjart, N., and de Laat, W. (2006). CTCF mediates long-range chromatin looping and local histone modification in the beta-globin locus. Genes Dev. *20*, 2349–2354.

Splinter, E., de Wit, E., van de Werken, H.J.G., Klous, P., and de Laat, W. (2012). Determining long-range chromatin interactions for selected genomic sites using 4C-seq technology: from fixation to computation. Methods *58*, 221–230.

Supek, F., Bošnjak, M., Škunca, N., and Šmuc, T. (2011). REVIGO summarizes and visualizes long lists of gene ontology terms. PLoS One *6*, e21800.

Tang, Z., Luo, O.J., Li, X., Zheng, M., Zhu, J.J., Szalaj, P., Trzaskoma, P., Magalska, A., Wlodarczyk, J., Ruszczycki, B., et al. (2015). CTCF-mediated human 3D genome architecture reveals chromatin topology for transcription. Cell *163*, 1611–1627.

UniProt Consortium (2015). UniProt: a hub for protein information. Nucleic Acids Res. *43*, D204–D212.

Walter, C., Schuetzmann, D., Rosenbauer, F., and Dugas, M. (2014). Basic4Cseq: an R/Bioconductor package for analyzing 4C-seq data. Bioinformatics *30*, 3268–3269.

van de Werken, H.J.G., Landan, G., Holwerda, S.J.B., Hoichman, M., Klous, P., Chachik, R., Splinter, E., Valdes-Quezada, C., Oz, Y., Bouwman, B.A.M., et al. (2012). Robust 4C-seq data analysis to screen for regulatory DNA interactions. Nat. Methods *9*, 969–972.

de Wit, E., Vos, E.S.M., Holwerda, S.J.B., Valdes-Quezada, C., Verstegen, M.J.A.M., Teunissen, H., Splinter, E., Wijchers, P.J., Krijger, P.H.L., and de Laat, W. (2015). CTCF binding polarity determines chromatin looping. Mol. Cell *60*, 676–684.

Yates, A., Beal, K., Keenan, S., McLaren, W., Pignatelli, M., Ritchie, G.R.S., Ruffier, M., Taylor, K., Vullo, A., and Flicek, P. (2015). The Ensembl REST API: Ensembl data for any language. Bioinformatics *31*, 143–145.

Yusufzai, T.M., Tagami, H., Nakatani, Y., and Felsenfeld, G. (2004). CTCF tethers an insulator to subnuclear sites, suggesting shared insulator mechanisms across species. Mol. Cell *13*, 291–298.

# STAR★METHODS

## KEY RESOURCES TABLE

| REAGENT or RESOURCE | SOURCE | IDENTIFIER |
|---|---|---|
| Chemicals, Peptides, and Recombinant Proteins | | |
| Dpn II enzyme (50,000 U/mL) | New England Biolabs | R0543M |
| Phusion High-Fidelity DNA polymerase | New England Biolabs | M0530S |
| Q5 High-Fidelity DNA polymerase | New England Biolabs | M0491S |
| QiaQuick PCR purification kit | Qiagen | 28104 |
| T4 DNA ligase HC 30 U / µL | ThermoFisher | EL0013 |
| Nla III enzyme (10,000 U/mL) | New England Biolabs | R0125L |
| Deposited Data | | |
| CTCF ChIP-seq 18 LCLs | Kasowski et al., 2013 | GEO: GSE50893 |
| RNA-seq 18 LCLs | Kasowski et al., 2013 | GEO: GSE50893 |
| PolII ChIP-seq 18 LCLs | Kasowski et al., 2013 | GEO: GSE50893 |
| H3K27ac ChIP-seq 18 LCLs | Kasowski et al., 2013 | GEO: GSE50893 |
| H3K4me1 ChIP-seq 18 LCLs | Kasowski et al., 2013 | GEO: GSE50893 |
| H3K4me3 ChIP-seq 18 LCLs | Kasowski et al., 2013 | GEO: GSE50893 |
| H3K36me3 ChIP-seq 18 LCLs | Kasowski et al., 2013 | GEO: GSE50893 |
| SA1 ChIP-seq 18 LCLs | Kasowski et al., 2013 | GEO: GSE50893 |
| Genotype 14 LCLs | 1000 Genomes project | http://www.internationalgenome.org/data |
| Rad21 ChIA-PET GM12878 | Grubert et al., 2015 | GEO: GSE62742 |
| H3K4me3 ChIA-PET GM12878 | Grubert et al., 2015 | GEO: GSE62742 |
| CTCF ChIA-PET GM12878 | Tang et al., 2015 | GEO: GSE72816 |
| HiC GM12878 | Rao et al., 2014 | GEO: GSE63525 |
| CHiC GM12878 | Mifsud et al., 2015 | E-MTAB-2323 |
| 4C-seq 6 LCLs | This study | ENA: PRJEB22940 |
| CAGE peaks human | FANTOM Consortium | http://fantom.gsc.riken.jp/5/datafiles/latest/extra/CAGE_peaks/ |
| Splicing QTLs LCLs | Li et al., 2016 | http://eqtl.uchicago.edu/jointLCL/ |
| Experimental Models: Cell Lines | | |
| Lymphoblastoid Cell Lines | Coriell Biorepository | cat.ID: GM12878; RRID: CVCL_7526, GM12891; RRID: CVCL_9633, GM12892; RRID: CVCL_9631, GM19238; RRID: CVCL_9633, GM19239; RRID: CVCL_9634 and GM19240; RRID: CVCL_9635 |
| Oligonucleotides | | |
| Primer: THRAP3 Forward:<br>AATGATACGGCGACCACCGAGATCT<br>ctaacttccatcagaggcgctcac | This study, Eurofins Genomics | N/A |
| Primer: THRAP3_i2 Reverse:<br>CAAGCAGAAGACGGCATACGAGATACATCG<br>attggcctggttcggtcttctc | This study, Eurofins Genomics | N/A |
| Primer: THRAP3_i4 Reverse:<br>CAAGCAGAAGACGGCATACGAGATTGGTCA<br>attggcctggttcggtcttctc | This study, Eurofins Genomics | N/A |
| Primer: THRAP3_i5 Reverse:<br>CAAGCAGAAGACGGCATACGAGATCACTGT<br>attggcctggttcggtcttctc | This study, Eurofins Genomics | N/A |
| Primer: THRAP3_i6 Reverse:<br>CAAGCAGAAGACGGCATACGAGATATTGGC<br>attggcctggttcggtcttctc | This study, Eurofins Genomics | N/A |

(*Continued on next page*)

**Continued**

| REAGENT or RESOURCE | SOURCE | IDENTIFIER |
|---|---|---|
| Primer THRAP3_i7 Reverse: CAAGCAGAAGACGGCATACGAGATGATCTG attggcctggttcggtcttctc | This study, Eurofins Genomics | N/A |
| Primer THRAP3_i12 Reverse: CAAGCAGAAGACGGCATACGAGATTACAAG attggcctggttcggtcttctc | This study, Eurofins Genomics | N/A |
| Software and Algorithms | | |
| R | The R Project | http://www.R-project.org/ |
| Bioconductor | Bioconductor | https://www.bioconductor.org/ |
| SNPhood | Arnold et al., 2016 | https://bioconductor.org/packages/SNPhood |
| PWMScan | PWMTools | http://ccg.vital-it.ch/pwmtools/pwmscan.php |
| Kallisto | Bray et al., 2016 | https://pachterlab.github.io/kallisto/ |
| DEXSeq | Anders et al., 2012 | https://bioconductor.org/packages/DEXSeq |
| intersectBed (Bedtools) | Quinlan and Hall, 2010 | http://bedtools.readthedocs.io/en/latest/content/tools/intersect.html |
| GenomicRanges | Lawrence et al., 2013 | https://bioconductor.org/packages/GenomicRanges |
| FastQC | Babraham bioinformatics | https://www.bioinformatics.babraham.ac.uk/projects/fastqc/ |
| Bowtie2 | Langmead and Salzberg, 2012 | http://bowtie-bio.sourceforge.net/bowtie2/index.shtml |
| ConsensusPathDB | Kamburov et al., 2013 | http://cpdb.molgen.mpg.de/ |
| Perl | Cunningham et al., 2015;<br>Yates et al., 2015 | https://www.perl.org/ |
| UNIPROT | UniProt Consortium | http://www.uniprot.org/ |
| Pfam | Bateman et al., 2004 | http://pfam.xfam.org/ |
| Revigo | Supek et al., 2011 | http://revigo.irb.hr/ |
| Chimera | Berman et al., 2000 | https://www.cgl.ucsf.edu/chimera/ |
| RCSB-PDB | RCSB-PDB | www.rcsb.org |
| dcGOR | Fang, 2014 | https://github.com/hfang-bristol/dcGOR |
| Basic4CSeq | Walter et al., 2014 | https://bioconductor.org/packages/Basic4CSeq |
| Other | | |
| GENCODE v19 | GENCODE | https://www.gencodegenes.org/releases/19.html |

## CONTACT FOR REAGENT AND RESOURCE SHARING

Further information and requests for resources, reagents, and code should be directed to and will be fulfilled by the Lead Contact, Judith B. Zaugg (judith.zaugg@embl.de).

## EXPERIMENTAL MODEL AND SUBJECT DETAILS

### Lymphoblastoid Cell Lines

Human lymphoblastoid cell lines obtained from B-lymphocytes were purchased from Coriell Biorepository, cat. ID: GM12878 (Female (F)), GM12891 (Male (M)), GM12892 (F), GM19238 (F), GM19239 (M) and GM19240 (F). Cells were cultured in RPMI 1640 medium with 30% Fetal Bovine Serum, 1 % penicillin and streptomycin (ThermoFisher) at 37°C 5% $CO_2$.

## METHOD DETAILS

### Annotation of Intragenic Loops

For the identification of CTCF peaks binding along transcripts, we defined four genic regions: promoter (+/- 1kb from transcription start site (TSS)), end of transcript (+/- 1kb of transcription termination site (TTS)), upstream, and downstream regions of exons (either 2 kb from outside the exon boundaries - when the intron was longer than 2kb - or the actual size of the intron in case it was shorter). We expect all promoters to fall within the TSS region and to avoid any overlaps between the promoter and exon regions, we removed any region associated with first exons, first introns and anything within 5kb from the TSS from the set of exonic regions. Additionally, we filtered out exons intersecting with CAGE peaks (FANTOM Consortium and the RIKEN PMI and CLST (DGT) et al., 2014) to prevent mis-classifying non-annotated promoters as exons.

To minimize the number of non-functional CTCF binding sites, we only considered sites that overlap with a CTCF peak in LCLs obtained from our previous study (Kasowski et al., 2013). We then intersected the CTCF peaks with each of these windows and assigned the highest scoring motif (MA0139.1) to each peak by using the PWMScan tool (http://ccg.vital-it.ch/pwmtools/pwmscan.php) (cut-off of 93.13% with non-overlapping matches). Motifs having a score of >= 500 (*LCL-specific set*) or >= 1000 were further used.

Given that CTCF binds to an asymmetric motif, it is possible to assign a directionality. We did so by defining directionality relative to the gene strand thus rendering *sense* CTCF motifs if both the motif and the gene lie in the same strand and *antisense* vice versa. We grouped the CTCF motif-pairs according to their genic region into: promoter:exon-upstream, promoter:exon-downstream, promoter-TTS, exon-upstream:TTS, and exon-downstream:TTS (schematic in Figure 1). We next classified the motif pairs based on their relative orientation to each other as "*convergent*", "*divergent*", "*both sense*", and "*both antisense*". For this analysis, we excluded any pair of motifs with a distance smaller than 5kb to allow for potential chromatin looping, and we only kept unique pairs.

### Overlap with Chromatin Conformation Data

For validation we overlapped the predicted loops with existing chromatin conformation data requiring that each motif of a CTCF motif-pair overlapped one side of the same interaction. We used cohesin subunit Rad21 and histone mark H3K4me3 ChIA-PET (Grubert et al., 2015), and CTCF (Tang et al., 2015) ChIA-PET and Capture Hi-C (CHiC) data (Mifsud et al., 2015). Briefly, CHiC uses oligonucleotides close to several promoters to amplify the reads obtained close to the TSS.

### Overlapping of CTCF Motifs with Splicing QTLs

Based on earlier studies suggesting that CTCF is capable of binding to sequences as long as 40-60bp (Li et al., 2013), we intersected a 40bp CTCF motif (+/-20bp from center of the canonical motif) with the list of splicing QTLs (sQTLs) (Li et al., 2016). We considered all sQTLs above an FDR of 10% as described in their methods.

### Identification of Differentially Used Exons

We obtained RNA-seq data (strand-specific and paired-end reads) for lymphoblastoid cell lines of 18 individuals from (Kasowski et al., 2013). We selected protein coding genes using the genome annotation provided in Gencode v19. We first filtered out lowly expressed isoforms as described in (Soneson et al., 2016) by applying the *kallisto* tool to all RNA-seq files (Bray et al., 2016), only keeping transcripts which were expressed in at least 10 out of the 18 individuals. We used custom scripts to generate a set of non-overlapping exon boundaries. This involved first splitting exons into individual parts (since some exons can be part of multiple transcripts and can have several annotated 5' and 3' boundaries) and then merging them again into units that contain the most 5' and the most 3' annotated boundary for each exon. Chromosomes X, Y and mitochondrial DNA were filtered out.

Based on current knowledge about exon length distribution (Derrien et al., 2012), we further removed exons that were less than 20 or more than 5,000bp long. These annotation and filtering steps resulted in a set of 109,960 exons. We then used *DEXSeq* (Anders et al., 2012) to count the reads falling into each of these exons for each of the replicates of the 18 individuals. As an additional filtering step, we excluded exons with less than 10 counts on average, leaving 86,285 exons for further processing (for a total of 9,198 genes) of which 62,663 (73%) were middle exons.

**D**ifferentially **U**sed **E**xons (DUEs) as described in (Anders et al., 2012), are defined as a change in exon usage whereby exon usage is defined as the ratio of reads mapping to a particular exon vs reads mapping anywhere else in a gene. To obtain the DUEs we used *DEXSeq* and compared the exon usage for each individual against the median across all the 18 individuals (Figure 2A). The such obtained log2 fold-change values were used for the correlation between exon and CTCF usage (see CTCF correlation with DUEs below). We considered exons to be differentially used when their adjusted p-value was below 0.1 (Benjamini Hochberg correction), leaving a total of 3,844 DUEs. In order to keep only the middle DUEs, exons were intersected with the TSS and TTS from the Gencode v19 annotation and respectively labelled as first, middle, and last exons. For further analysis, we excluded the first and last exons, considering only the 2,081 middle DUEs.

These DUEs cover 14% (1148) of expressed genes with multiple exons. From these 1148 genes, most have less than 10 DUEs (Figure S2A), and no strong correlation between the number of middle exons per gene and number of differentially used exons was observed (Figure S2B). The size distribution of DUEs is similar to the overall size distribution of exons and consistent with previous observations (Derrien et al., 2012) (Figure S2C).

### CTCF Correlation with DUEs

To calculate the log2 fold-change per exon in each of the individuals against the median expression based on their *DEXSeq* counts, we estimated the exon fold-changes as described above and in (Anders et al., 2012). As a quality control, we checked the distribution of fold-changes with respect to the median for each individual and found that it shows similar patterns for all of them (Figure S2D).

For the quantification of the ChIP-seq read counts of CTCF and RNA PolII binding around the exons, we used *SNPhood* (Arnold et al., 2016). We extracted the reads of CTCF falling within 2kb downstream or upstream of the 5' and 3' boundaries of exons respectively. We then calculated the log2 fold-change of CTCF counts between each individual and the median individual, similar as described for the RNA-seq data. These fold-changes were then correlated with the fold-changes of the exon.

The same procedure was applied to other genomic features (PolII, SA1, H3K4ME1, H3K4ME3, H3K36ME3, H3K27AC) from paired data (Figure S2F). Note that only cases where the median factor read counts were 10 or more were considered. For each exon, we generated 100 sets of permutations for fold-changes in exon usage between individuals, keeping the number of individuals with positive and negative fold-change constant at each exon. This empirical distribution was then used to assess the significance of the correlations by applying Wilcoxon tests.

## Allele Specific Analysis of CTCF Binding

We first extracted all heterozygous SNPs from the genotypes of the 14 individuals (1000 Genomes project), for which genotypes were available, and intersected them with the CTCF peaks from the ChIP-seq data. 80% of all the peaks (158,455) contained 1 or more heterozygous SNPs in at least one individual. We then kept the SNPs closest to the midpoint of the motif that was predicted to form an intragenic interaction.

Using *SNPhood*, we analysed whether there was an allelic bias for the read counts extracted in the region of +/- 250 bp surrounding the SNP. Briefly, *SNPhood* performs a binomial test to assess whether the allelic fractions are deviating from the expected 0.5. We selected all CTCF peaks within 2kb upstream or downstream of an exon boundary that overlapped with a heterozygous SNP in at least one individual, calculated the allelic bias and filtered the peaks based on a nominal p-value cutoff of 0.05, which resulted in a set of 9,434 upstream and 7,689 downstream allele-specific bound CTCF peaks. This set of peaks served as a basis for the correlation with exon allelic bias.

To calculate the allelic bias for exons, we split the RNA-seq alignment files by allele to which they map (allele information was obtained from (Kasowski et al., 2013)) using samtools split and then used bedtools (intersectBed) (Quinlan and Hall, 2010) to extract the counts. To assess exon allelic bias we performed a binomial test that resulted in 1,327 and 664 events upstream and downstream respectively (at nominal p-value < 0.05). To avoid low-count artefacts, we only kept SNPs that had at least 5 mean read counts.

To verify whether there was an enrichment of allele specific CTCF binding in the 2kb upstream or downstream of the exons, we identified middle exons that overlap with CTCF peaks using *GenomicRanges*. Only those cases where the individual was heterozygous for the SNP and both CTCF and exon were allele specific were taken into account. As described in the main text, to obtain a more robust quantification we classified the exons according to the directionality of the allelic bias in CTCF binding and assessed differences in exon allelic fractions between the two groups by a t-test (bottom panel Figures 3A and S3A). This revealed a significant association only for the CTCF sites upstream of the exon.

For the genome-wide correlation of HiC signal with CTCF binding in an allele specific manner, we used the GM12878 diploid HiC maps at 5kb resolution (Rao et al., 2014) and the CTCF and exon counts as mentioned above. We calculated normalised interaction frequencies with Knight-Ruiz normalisation vectors and we followed the same procedure described by the authors in their supplemental methods. We obtained the allelic fraction by calculating the ratio of maternal counts with respect to the total counts. Next, we selected the CTCF peaks binding in +/-2kb from all middle exons that contained SNPs for which GM12878 was heterozygous. We finally stratified either the CTCF or the exon allelic fraction based on the HiC allelic fraction as described above (Figure S3B).

## 4C-Seq Experiments

4C-seq was performed using 6 human LCLs (see Experimental Model and Subject Details). The protocol was modified from (van de Werken et al., 2012). All chemicals and reagents were purchased from Sigma Aldrich unless otherwise stated in brackets. To perform crosslinking of chromatin, 10 million cells per cell line were fixed in 5 mL 2% formaldehyde (VWR) at room temperature for 10 minutes. 250 μL of 2.5 M glycine was added to quench the crosslinking reaction for 3 minutes at room temperature. Cells were washed twice in ice cold PBS and were snap frozen using liquid nitrogen prior to 4C experiments.

To perform in nucleus Dpn II restriction digest of crosslinked genomic DNA, 10 million cells per cell line were first lysed in 5 mL lysis buffer [10 mM pH 7.5 Tris-HCl, 10 mM NaCl, 0.2% NP-40, 1X complete EDTA-free protease inhibitor (Roche)] for 30 minutes on ice. Nuclei were centrifuged at 600 rcf for 6 minutes at 4°C. Supernatant was discarded and the nuclei were then resuspended in 1 mL residual supernatant. The samples were then centrifuged again at 600 rcf for 6 minutes at 4°C and the supernatant was discarded. The nuclei pellets were washed in 200 μL of 1.25X Dpn II Buffer (NEB) without resuspension at 600 rcf for 1 minute at 4°C. The nuclei pellets were then resuspended gently in 492.5 μL of 1.25X Dpn II Buffer with 0.3% sodium dodecyl sulfate. The mixture was incubated at 37°C and 950 rpm in a thermomixer (Eppendorf) with heated lid for 1 hour. 50 μL 20% Triton X-100 was then added to the mixture and was further incubated for 1 hour at 37°C and 950 rpm. Dpn II restriction digest was then performed by the addition of 45 μL nuclease free water (Ambion) and 10 μL DpnII enzyme (NEB), and the reaction was incubated at 37°C and 950 rpm for 3 - 5 hours with heated lid in the thermomixer. An addition 10 μL of DpnII was added to the mixture and was further incubated in the thermomixer overnight.

To ligate digested DNA for generating a 3C template, the mixture was heat inactivated for 20 minutes at 65°C, followed by centrifugation at 600 rcf for 6 minutes at 4°C. Supernatant was removed, leaving 50 μL. Ligation reaction mixture of 950 μL [50 mM pH 7.5 Tris-HCl, 10 mM $MgCl^2$, 1 mM ATP (NEB) and 5 mM dithiolthreitol, 0.1 μg/μL bovine serum albumin (NEB) and 150 U/μL T4 DNase ligase HC (ThermoFisher)] was added to the samples and was incubated overnight at 16°C and 600 rpm in the thermomixer.

To reverse crosslink, the samples were incubated with 200 mg proteinase K (ThermoFisher) and 50 μL 20% sodium dodecyl sulfate at 65°C for 1 hour. The samples were then incubated with 100 mg RNase A (Qiagen) for 45 minutes at 37°C.

To purify the 3C template, a phenol chloroform extraction method was performed where 1 volume of phenol:chloroform:isoamyl alcohol 25:24:1 saturated with 10 mM Tris pH 8.0, 1 mM EDTA was added to the samples and were mixed thoroughly by vortexing. The mixture was transferred to a 2 mL heavy phase lock gel tube (5-Prime) and was centrifuged at 16,000 rcf for 5 minutes at room temperature. The top clear aqueous phase containing DNA was transferred to a clean eppendorf. NaCl of a final concentration of 200 mM, together with 1 μL of 20 μg/μL glycogen was added to the aqueous DNA solution, followed by the addition of 2 volume of -20°C 100% ethanol. The mixture was incubated at -80°C for at least 1 hour and was centrifuged at 15,000 rpm for 1 hour at 4°C. The supernatant was removed and 500 μL -20°C 80% ethanol was added to wash the DNA pellet at 15,000 rpm for 60 minutes at 4°C. The supernatant was then removed and the tubes were centrifuged again for 30 minutes at 15,000 rpm at 4°C. The residual supernatant was then removed and the DNA pellet was allowed to be air dried for 5 minutes at room temperature. To resuspend DNA, 50 μL 65°C 10 mM pH 7.5 Tris-HCl was added to the DNA pellet and the solution was incubated at 65°C for 5 minutes to dissolve the pellet. Digestion and ligation efficiencies were determined by agarose gel electrophoresis.

To perform the 2nd round of restriction digestion with NlaIII enzyme (NEB), 5 μL 10 U/μL NlaIII and 6 μL 10X NlaIII buffer (NEB) was added to 50 μL 3C template, and the reaction was incubated at 37°C overnight. NlaIII was heat inactivated at 65°C for 20 minutes.

To generate 4C template, 5X ligation buffer [250 mM Tris-HCl, 50 mM $MgCl_2$, 5 mM ATP, 25 mM dithiolthreitol], 5 μL 10 mg/mL bovine serum albumin (NEB) and 2.5 μL 150 U/μL T4 DNase ligase HC (ThermoFisher) were added to 50 μL NlaIII digested 3C template and the reaction was incubated overnight at 16°C.

To purify 4C DNA template, DNA purification was performed as described above. The final 4C template was further purified using the QIAquick PCR purification kit (Qiagen) according to the manufacturer's instruction. Digestion and ligation efficiencies were assessed by agarose gel electrophoresis.

To design primers for performing 4C-PCR, the viewpoint sequence of the *THRAP3* gene was first chosen using *THRAP3* sequence obtained from the UCSC genome browser (https://genome.ucsc.edu/index.html) on the human GRCh37/hg19 assembly. Restriction site identification and *THRAP3* sequence were processed using ApE-A plasmid editor (http://biologylabs.utah.edu/jorgensen/wayned/ape/). 4C-PCR primers were designed using primer3 v. 0.4.0 (http://bioinfo.ut.ee/primer3-0.4.0/). Viewpoint and primer sequences were chosen and designed, respectively, according to the guidelines as previously published (Splinter et al., 2012.). Viewpoint coordinate correspond to the human GRCh37/hg19 assembly chr1:36690087-36690526. The forward and reverse primer sequences are 5' ctaacttccatcagaggcgctcac 3' and 5' attggcctggttcggtcttctc 3' respectively. Illumina adapters and indexing sequences were incorporated into the PCR primers. High-performance liquid chromatography purification was used in the production of primers (Eurofins Genomics). The primer sequences (5' to 3') can be found in the Key Resources Table. Oligonucleotide sequences copyright 2016 Illumina. All rights reserved. Derivative works created by Illumina customers are authorized for use with Illumina instruments and products only. All other uses are strictly prohibited.

To perform 4C-PCR, 4C template from each of the 6 individuals were amplified using primers above, with each index assigned to 1 individual. 4C-PCR was performed with the following condition:

| Temperature (°C) | Time (sec) | Cycle |
|---|---|---|
| 98 | 30 | 1 |
| 98 | 10 | 30 |
| 68 | 30 | |
| 72 | 180 | |
| 4 | 30 | 1 |

For each individual, two 4C-PCRs were pooled together and the PCR products were purified using Agencourt AMPure XP beads (Beckman Coulter) according to the manufacturer's instruction. 4C-seq library was prepared by pooling equimolar amounts of the barcoded 4C templates. Sequencing was performed on the MiSeq platform with 75 bp read length for single end reads. Custom sequencing [5' actcacctgggcctaccacagagatc 3'] and indexing [5' gagaagaccgaaccaggccaat 3'] primers were used. Two technical replicates were performed for all individuals.

### 4C-Seq Data Analysis

To process raw 4C-seq data, FastQC was used to verify that all libraries passed the quality controls (https://www.bioinformatics.babraham.ac.uk/projects/fastqc/). Adapter trimming was not required as sequencing began at the first base after the DpnII site. Sequencing reads were aligned to hg19 using Bowtie2 (Langmead and Salzberg, 2012) with parameters: -p 8, –very-sensitive, –time. Only reads with a MAPQ score >= 10 were used.

The processed data were then analysed using the bioconductor package *Basic4CSeq* according to the author's instructions (Walter, C., 2015). Briefly, the restriction fragments were simulated *in silico* and aligned sequencing reads were mapped to the restriction fragments. Fragment read count was normalised to reads per million (RPM), and 4C interaction was subsequently visualised. We observed a cis (0.2 Mb region adjacent to the viewpoint) to overall reads ratio of about 40% in all of the 4C-seq experiments performed. A cis to overall ratio of 40% or above is considered as a quality control point for 4C experiments (van de Werken et al., 2012), indicating our 4C experiments achieved the recommended quality. 4C interactions were then visualised as a plot of normalised read count versus genomic coordinates.

To study the relation between 4C signals and differential exon usage of the 6 individuals, the bioconductor package GenomicRanges (Lawrence et al., 2013) was used to overlap normalised 4C read counts and CTCF peak signals. 4C reads mapped to fragment ends that overlap a plus and minus +/- 1kb region of the mid point of the CTCF peaks were considered to be a readout for the CTCF peak's interaction with the viewpoint CTCF. The 4C readout signals was representing CTCF interactions were then stratified by the relative inclusion and exclusion of the exon usage to generate the box plot.

### Functional Analyses

As mentioned in the text, two sets of exons were considered for the analyses: the *unbiased* and the *LCL-specific* set of looped exons. For the *unbiased* set the intragenic loops were annotated for cases where the CTCF motif score was >= 1000; this set reflects the potential of genes to form promoter- exon loops in any given tissue - as the identified loops were based only in the motifs. The *LCL-specific* set is defined above (Annotation of intragenic loops) and represents a subset of the *unbiased set*, showing CTCF binding and exon expression in LCLs, along with >= 500 score for the motifs and +/- 1kb for the TSS window.

All exon coordinates were used to retrieve the protein information from Ensembl with the assistance of Perl APIs (Cunningham et al., 2015; Yates et al., 2015). Different features on the retrieved protein regions were mapped using the Uniprot features of the corresponding protein (UniProt Consortium, 2015). Protein domains on the sequence were mapped using a local installation of Pfam (Bateman et al., 2004).

Gene Ontology (GO) term analysis for looping genes was performed using ConsensusPathDB webserver (CPDB) (http://consensuspathdb.org/) (Kamburov et al., 2013). The top 10 GO terms were visualized using Revigo (Supek et al., 2011) and represented as treemaps. All the statistical tests were done in R. The Pfam domain-to-GO term analysis was performed with the dcGOR R package (Fang, 2014). Location of exons on the primary sequence is based on the protein feature view from RCSB-PDB (www.rcsb.org). Domain definitions are based on the Pfam. The structure visualization and rendering was done with the help of the UCSF Chimera package (Berman et al., 2000).

## QUANTIFICATION AND STATISTICAL ANALYSIS

Most of the analyses were done using R (http://www.R-project.org/) and Bioconductor (https://www.bioconductor.org/), in particular using the *SNPhood* (Arnold et al., 2016) *DEXSeq* (Anders et al., 2012), and *GenomicRanges* (Lawrence et al., 2013) packages. Significance of the statistical analyses was calculated either with Fisher's exact test, Wilcoxon test, Binomial test, or t-test. For correlations, Pearson's R and Spearman rho were used as indicated. The choice of test, the p value thresholds, and the value of n are described for each analysis within the main manuscript, the method details, and in the figure legends. Permutations were obtained by randomly assigning the sample labels.

## DATA AND SOFTWARE AVAILABILITY

Raw and processed data for the 4C-seq libraries has been deposited in the European Nucleotide Archive under the accession-number PRJEB22940. Scripts are available upon request.